Supporting information

Vanadium Dioxide-Reduced Graphene Oxide Binary Host as an Efficient Polysulfide Plague for High Performance Lithium Sulfur Batteries

Sha Li[1], Yuan Cen[1], Qin Xiang, Muhammad Kashif Aslam, Bingbing Hu, Wei Li, Ya Tang, Qi Yu, Yuping Liu* and Changguo Chen*

College of Chemistry and Chemical Engineering, Chongqing University, Chongqing 401331, China.

Equal Contribution[1]

AUTHOR INFORMATION

Corresponding author:

Name: Changguo Chen

Tel: +86 13608357956

E-mail: cgchen@cqu.edu.cn (C.G. Chen)

Name: Yuping Liu

Tel: +86 13594157660

E-mail: liuyuping@cqu.edu.cn

Notes

The authors declare no competing financial interest.

Figure captions

Fig. S1. EDX spectrum (a), STEM image (b) and corresponding elemental mapping (c-d) of the pure VO_2.

Fig. S2. EDX spectrum (a); SEM image (b) and corresponding elemental mapping (c-f) of the VO_2@rGO/S composite

Fig. S3. Raman spectra of the pure VO_2 (a); XRD patterns of VO_2@rGO-2 binary host (b), VO_2@rGO/S composite (c) and TGA curves of VO_2@rGO/S, rGO/S and S in N_2 atmosphere (d).

Fig. S4. UV−vis absorption spectra of Li_2S_6/DME&DOL solution with the pure VO_2 and rGO, with the inset showing visualized adsorption of blank Li_2S_6/DME&DOL solutions and Li_2S_6/DME&DOL solutions with the VO_2 and rGO, respectively.

Fig. S5. Cross-sectional SEM image of the VO2@rGO/S electrode with different sulfur loading at (a) around 1.5 mg cm^{-2} and (b) around 4 mg cm^{-2}.

Fig. S6. (a) DualScope MP0R thickness gauge of the principles; (b) The standard card; The thickness of the VO_2@rGO/S electrode with different sulfur loading at (c) around 1.5 mg cm^{-2} and (d) around 4 mg cm^{-2}.

Fig. S7. The comparison of peak potentials (a) and corresponding onset voltages (b) of the VO_2@rGO/S, rGO/S and VO_2/S composites; CV profiles of rGO/S (c) and VO_2/S (d) composites at various scan rates; Cathodic one (e) and two (f) currents of the VO_2@rGO/S, rGO/S and VO_2/S composites and their corresponding the square root of scan rates.

Fig. S8. Charge-discharge voltage profiles (a) and Cycle performance (b) of the pure VO_2 in the same electrolyte within the voltage window of 1.7-2.8 V for LSBs system.

Fig. S9. (a) Comparison of the rate capacities and capacity retentions of the VO_2@rGO/S, rGO/S and VO_2/S composites; Galvanostatic charge/discharge profiles of the VO_2@rGO/S (b), rGO/S (c) and VO_2/S (d) composites at various rates.

Fig. S10. (a)Galvanostatic charge/discharge profiles of the VO_2@rGO/S composite at at 1 C; (b) CV curves (0.1 mV s^{-1}) of the VO_2@rGO/S and VO_2@rGO/S-2 composites; (e) Long-term cycling performance and Coulombic efficiency of the

VO_2@rGO/S-2 at 3 C; (d) EIS Nyquist plots of the VO_2@rGO/S, rGO/S, VO_2/S and VO_2@rGO/S-2 composites before initial discharge, the inset is equivalent circuit of fresh cells; (e) The application of VO_2@rGO/S electrode, powering 20 light-emitting diodes.

Fig. S11. (a) The cycling performance of the VO_2@rGO/S cathode with 4 mg cm^{-2} sulfur loading at a current density of 0.335 mA $cm^{-2}$and 3.35 mA cm^{-2}; (b) The corresponding charge-discharge profile on 1^{st}, 2^{nd}, 10^{th}, 20^{th} cycle, respectively.

Fig. S12. SEM images of VO_2@rGO/S and rGO/S (a,c) fresh and (b,d) cycled cathode at 1C.

Table S1

A comparison of electrochemical performance of VO_2@rGO/S composite between this work and some other cathode materials for LSBs in published literatures.

Table S2

Electrode Resistance Obtained from the Equivalent Circuit Fitting of the VO_2@rGO/S, rGO/S, VO_2/S and VO_2@rGO/S-2 composites before initial discharge.

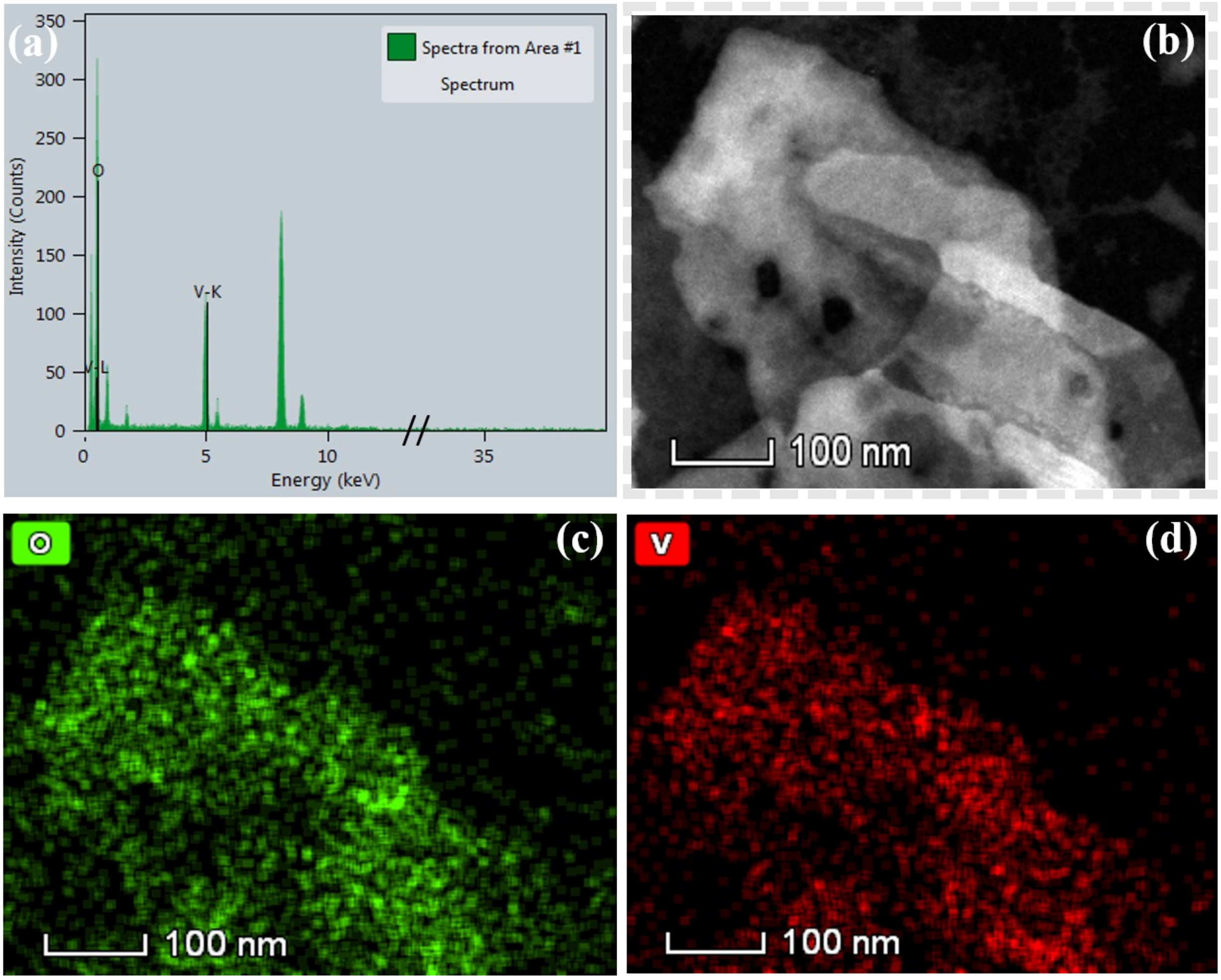

Fig. S1. EDX spectrum (a), STEM image (b) and corresponding elemental mapping (c-d) of the pure VO_2.

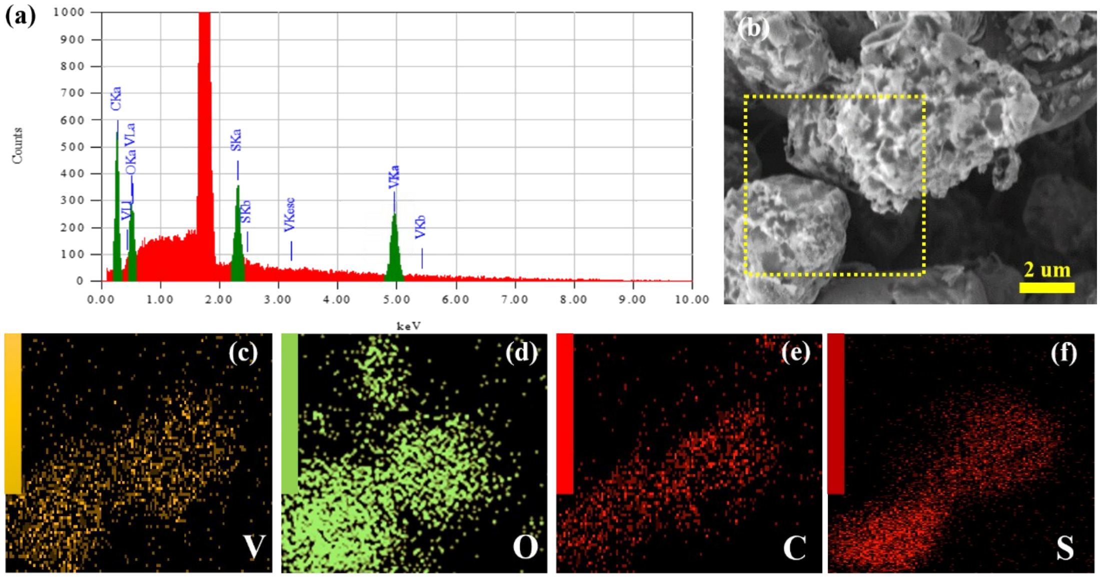

Fig. S2. EDX spectrum (a); SEM image (b) and corresponding elemental mapping (c-f) of the VO_2@rGO/S composite

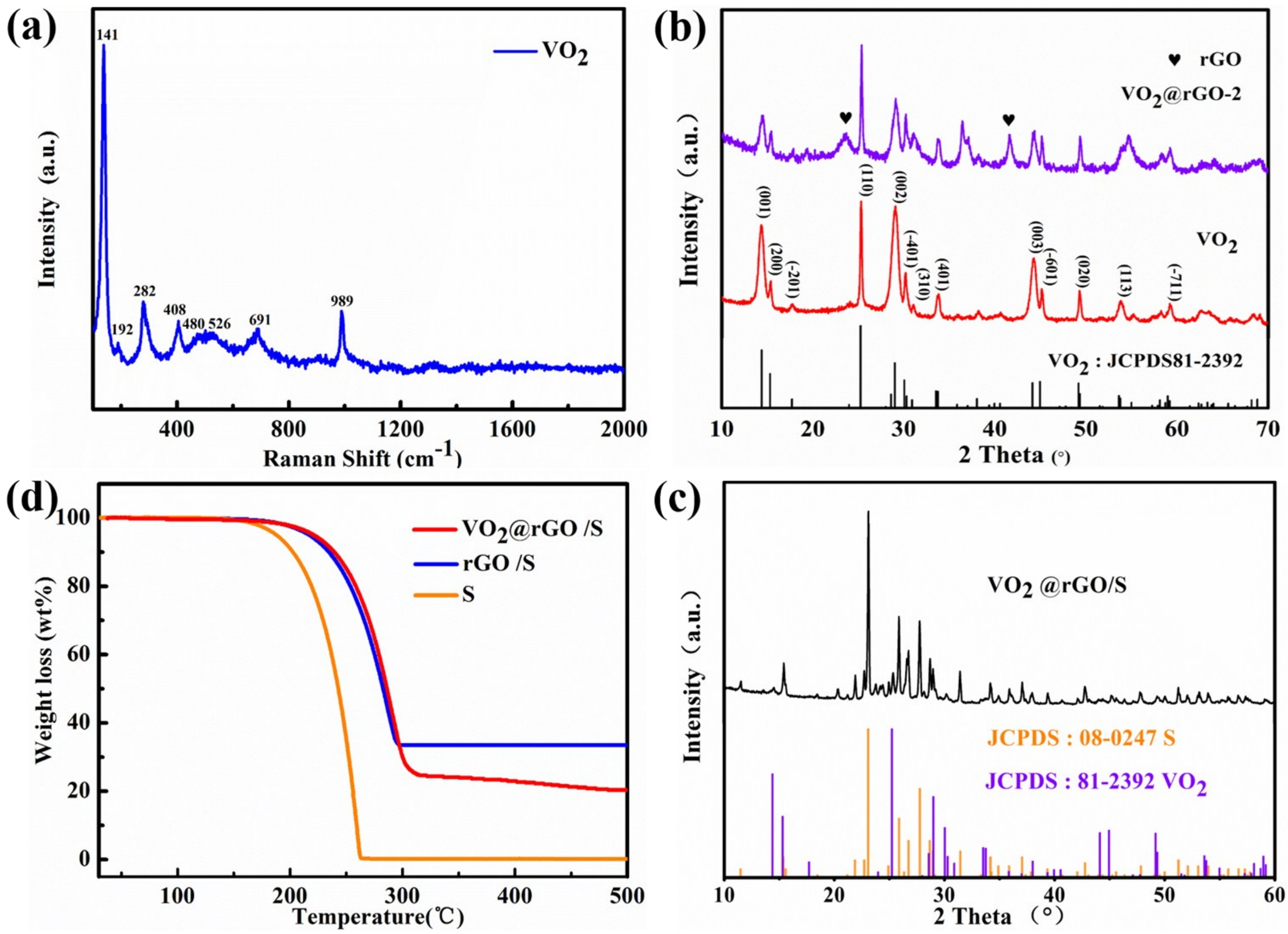

Fig. S3. Raman spectra of the pure VO_2 (a); XRD patterns of VO_2@rGO-2 binary host (b), VO_2@rGO/S composite (c) and TGA curves of VO_2@rGO/S, rGO/S and S in N_2 atmosphere (d).

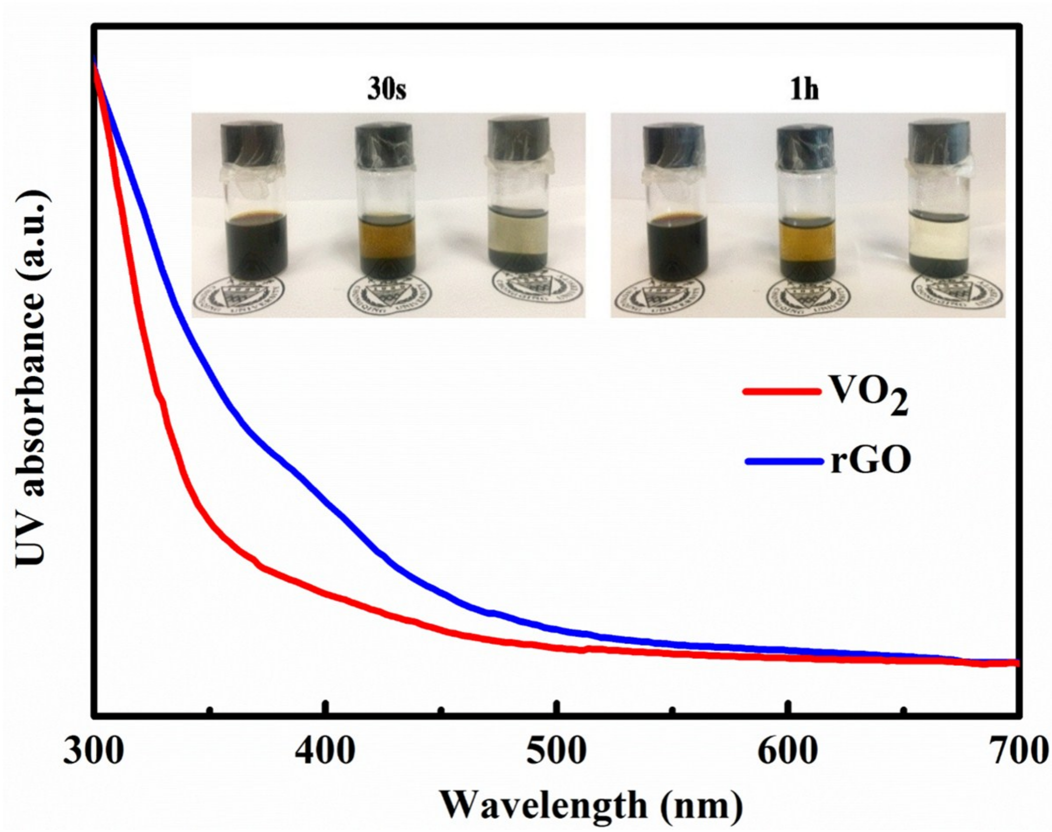

Fig. S4. UV−vis absorption spectra of Li_2S_6/DME&DOL solution with the pure VO_2 and rGO, with the inset showing visualized adsorption of blank Li_2S_6/DME&DOL solutions and Li_2S_6/DME&DOL solutions with the VO_2 and rGO, respectively.

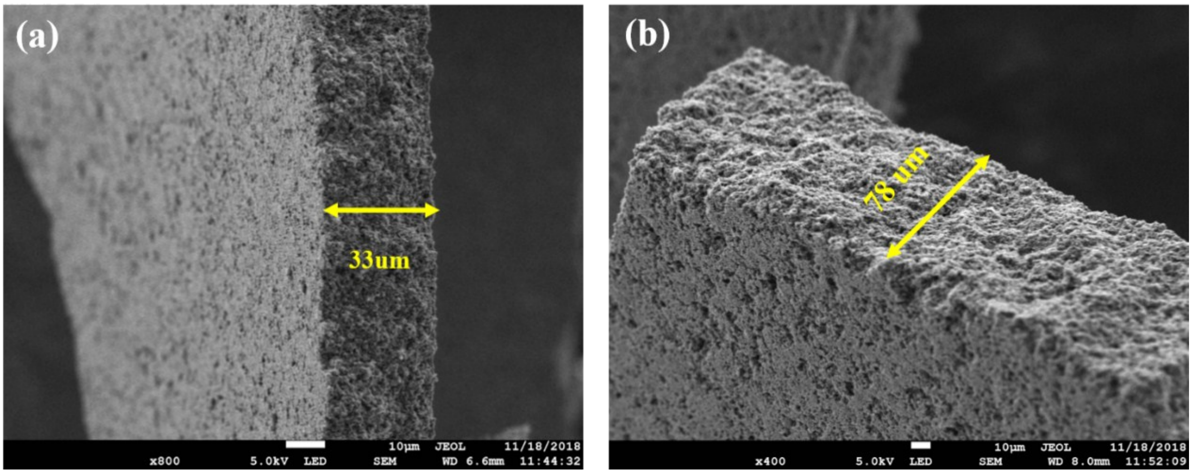

Fig. S5. Cross-sectional SEM image of the VO2@rGO/S electrode with different sulfur loading at (a) around 1.5 mg cm^{-2} and (b) around 4 mg cm^{-2}.

Fig. S6. (a) DualScope MP0R thickness gauge of the principles; (b) The standard card; The thickness of the VO_2@rGO/S electrode with different sulfur loading at (c) around 1.5 mg cm^{-2} and (d) around 4 mg cm^{-2}.

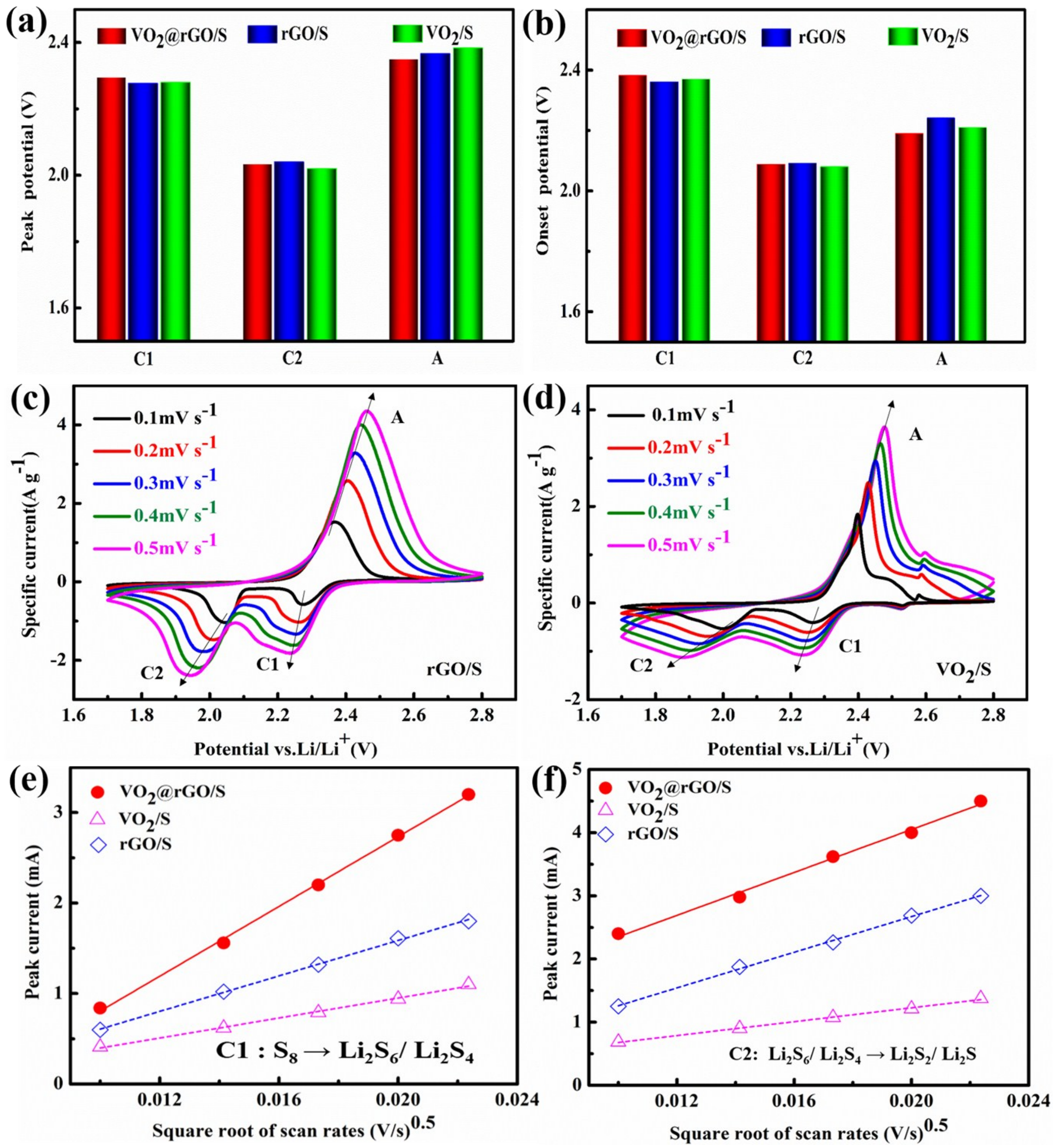

Fig. S7. The comparison of peak potentials (a) and corresponding onset voltages (b) of the VO_2@rGO/S, rGO/S and VO_2/S composites; CV profiles of rGO/S (c) and VO_2/S (d) composites at various scan rates; Cathodic one (e) and two (f) currents of the VO_2@rGO/S, rGO/S and VO_2/S composites and their corresponding the square root of scan rates.

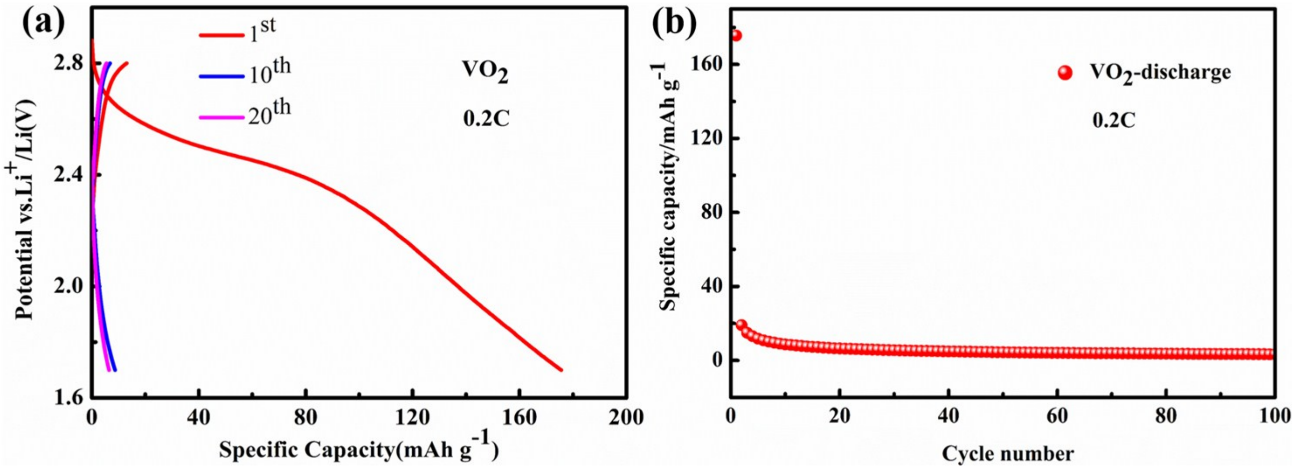

Fig. S8. Charge-discharge voltage profiles (a) and Cycle performance (b) of the pure VO_2 in the same electrolyte within the voltage window of 1.7-2.8 V for LSBs system.

As is well known, although the VO_2 with good electrochemical performance used as a lithium storage material was reported in LIBs,[15-18] the electrolytes are the critical role for their corresponding energy storage systems. In LIBs, the electrolyte is ethylene carbonate, not ethers electrolytes, which have been seriously hampered by high working voltage.

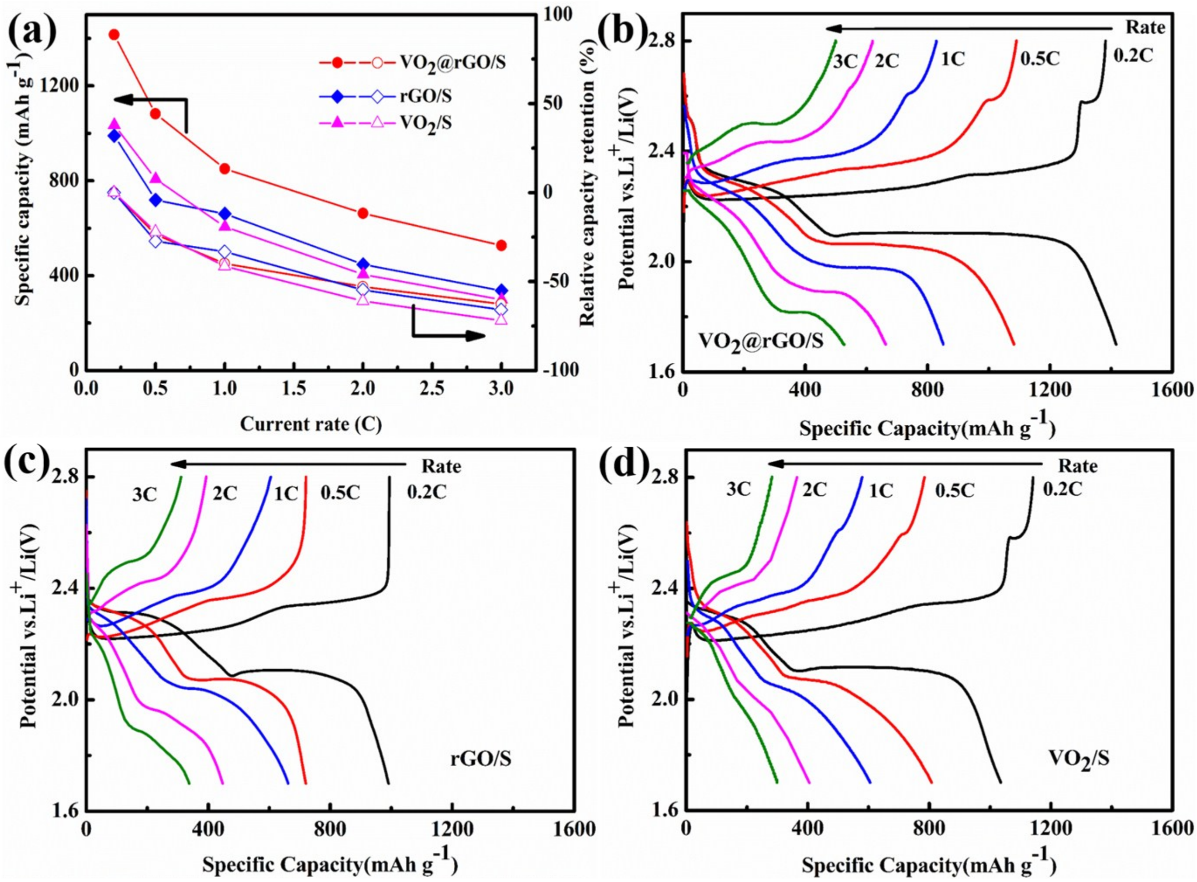

Fig. S9. (a) Comparison of the rate capacities and capacity retentions of the VO_2@rGO/S, rGO/S and VO_2/S composites; Galvanostatic charge/discharge profiles of the VO_2@rGO/S (b), rGO/S (c) and VO_2/S (d) composites at various rates.

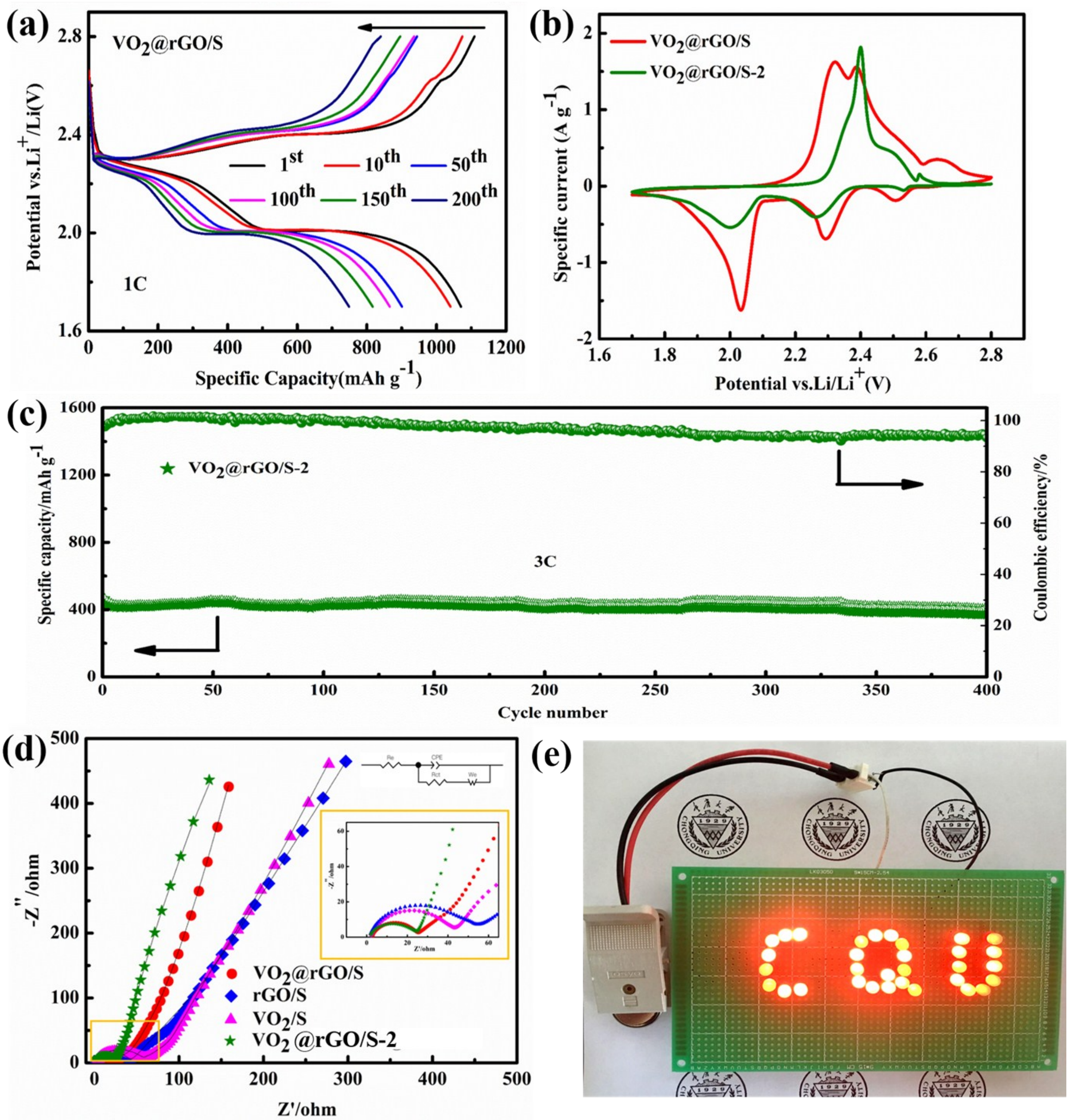

Fig. S10. (a) Galvanostatic charge/discharge profiles of the VO_2@rGO/S composite at at 1 C; (b) CV curves (0.1 mV s^{-1}) of the VO_2@rGO/S and VO_2@rGO/S-2 composites; (e) Long-term cycling performance and Coulombic efficiency of the VO_2@rGO/S-2 at 3 C; (d) EIS Nyquist plots of the VO_2@rGO/S, rGO/S, VO_2/S and

VO_2@rGO/S-2 composites before initial discharge, the inset is equivalent circuit of fresh cells; (e) The application of VO_2@rGO/S electrode, powering 20 light-emitting diodes.

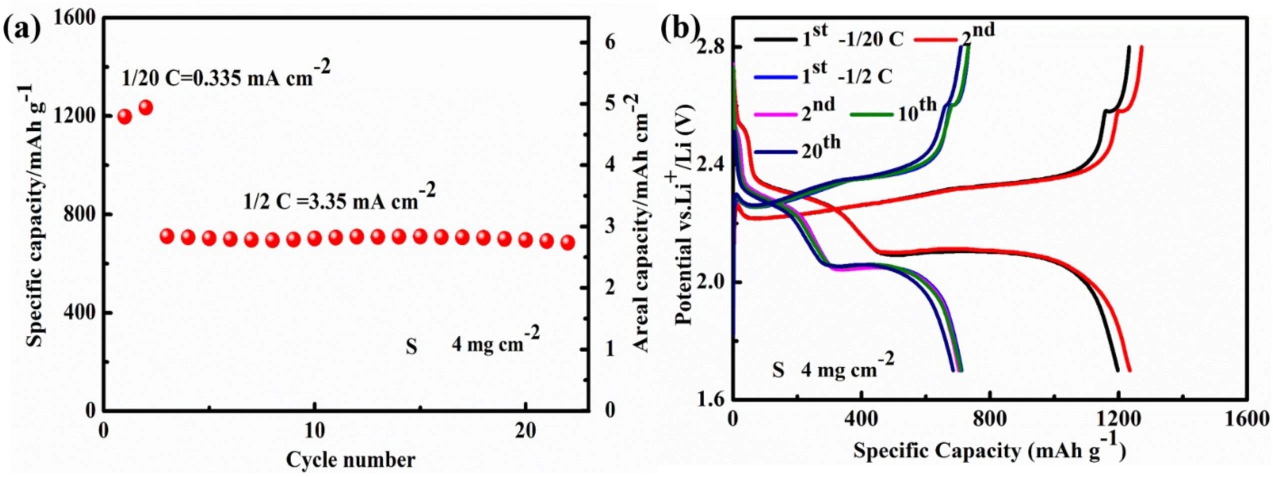

Fig. S11. (a) The cycling performance of the VO_2@rGO/S cathode with 4 mg cm^{-2} sulfur loading at a current density of 0.335 mA $cm^{-2}$and 3.35 mA cm^{-2}; (b) The corresponding charge-discharge profile on 1^{st}, 2^{nd}, 10^{th}, 20^{th} cycle, respectively.

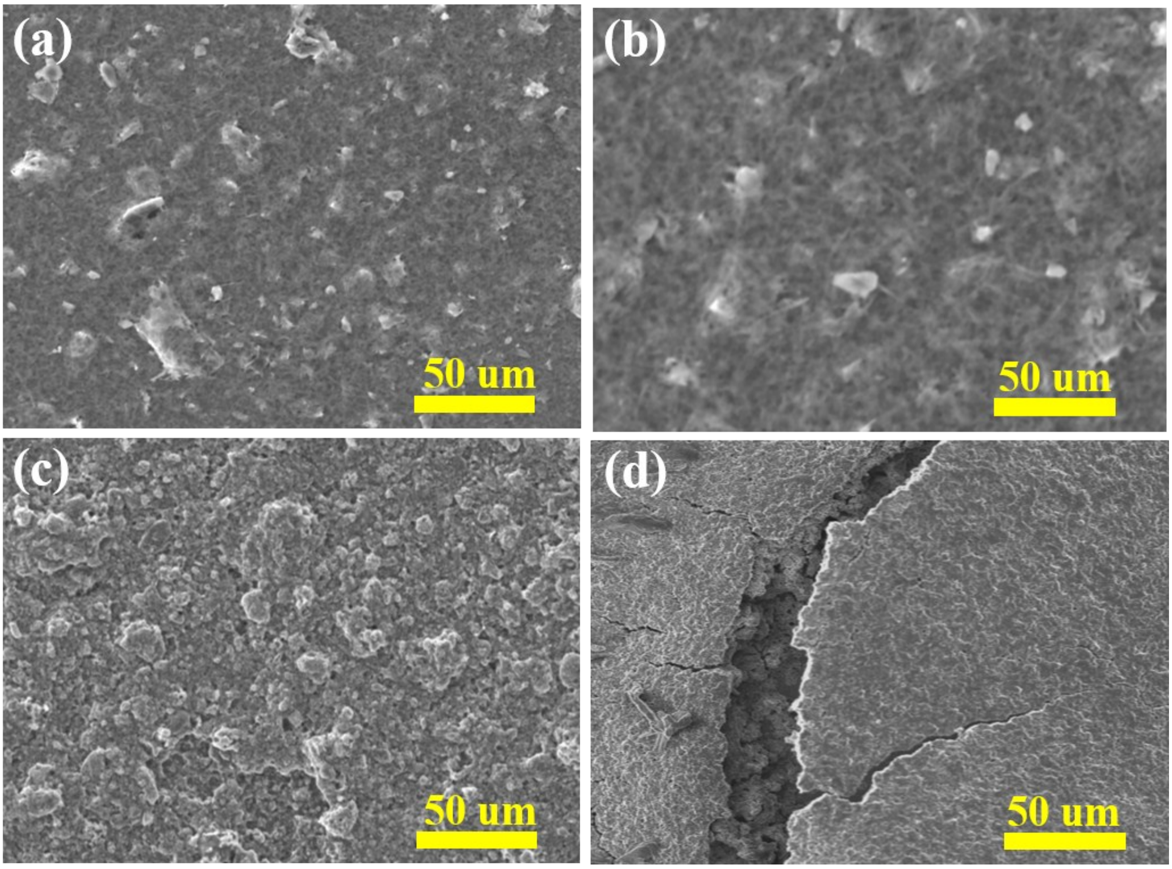

Fig. S12. SEM images of VO_2@rGO/S and rGO/S (a,c) fresh and (b,d) cycled cathode at 1C.

Table S1

A comparison of electrochemical performance of VO_2@rGO/S composite between this work and some other cathode materials for LSBs in published literatures.

Cathode Materials	Sulfur Loding (wt%)	Rate (C)	Discharge Capacity (mAh g^{-1})	Capacity after cycling	Ref.
VO_2/G/S	70	0.2	1405	990(100th)	1
TiO_2 /rGO/S	60	0.2	~1200	666(300th)	2
S/SnO_2@C	58	200 mA/g	1473.1	764 (100th)	3
PPy@MnO2@S	74.25	0.2	1372	964(200th)	4
V_2O_5/C/S	～	0.2	1520	940(50th)	5
VO_2@rGO/S	76.1	0.2	1358	1049(370th)	this work

Table S2

Electrode Resistance Obtained from the Equivalent Circuit Fitting of the VO_2@rGO/S, rGO/S, VO_2/S and VO_2@rGO/S-2 composites before initial discharge.

Sample	Re(Ω)	Rct	We
VO_2@rGO/S	2.7	22.0	1065
VO_2/S	0.5	58.9	2056
rGO/S	1.9	40.2	1937
VO_2@rGO/S-2	0.7	24.4	1024

References

1. Y. Song, W. Zhao, X. Zhu, L. Zhang, Q. Li, F. Ding, Z. Liu and J. Sun, *ACS Appl Mater Interfaces*, 2018, **10**, 15733-15741.
2. J. Song, J. Zheng, S. Feng, C. Zhu, S. Fu, W. Zhao, D. Du and Y. Lin, *Carbon*, 2018, **128**, 63-69.
3. Y. Li, B. Shi, W. Liu, R. Guo, H. Pei, D. Ye, J. Xie and J. Kong, *Electrochimica Acta*, 2018, **260**, 912-920.
4. B. Cao, Li, B. Hou, Y. Mo, L. Yin and Y. Chen, *ACS Appl Mater Interfaces*, 2016, **8**, 27795–27802.
5. M.-S. Kim, E. S. Shin, J.-S. Kim, W. I. Cho and S. H. Oh, *Journal of Electroceramics*, 2014, **33**, 142-148.